Electronic Supplementary Information

Thermogalvanic energy harvesting from forced convection cooling of 100–200 °C surfaces generating high power density

Yutaka Ikeda,[a] Yuki Cho[a] and Yoichi Murakami[a,b]*

[a] School of Engineering, Tokyo Institute of Technology, 2-12-1 Ookayama, Meguro, Tokyo 152-8552, Japan.

[b] PRESTO, JST, 4-1-8 Honcho, Kawaguchi, Saitama 332-0012, Japan.

*Corresponding Author: Yoichi Murakami, E-mail: murakami.y.af@m.titech.ac.jp

List of Contents

Simulation details

All of the numerical simulations were performed using ANSYS Fluent software (version 2020 R1). The number of meshes was chosen to be sufficiently high (ca. 3.7 million meshes) and the maximum mesh skewness in the simulation domain was suppressed below 0.9 to ensure reliable simulations. To properly simulate the boundary layers, seven layers of the inflation mesh, which were thin rectangular meshes suitable for representing boundary layers, were placed on all of the liquid-contacting surfaces inside the cell. To include the effect of buoyancy, the gravity force and the temperature dependence of the density of the electrolytes were considered. For the latter, we applied the reported slope[S1] of the decrement of the density of GBL with temperature to the densities of the present electrolytes measured by us at room temperature. The temperature dependence of η was considered using the VFT parameters (see the Experimental section in the main text), and that of c_p was considered using the parameters obtained by fitting the experimentally measured temperature dependence of c_p (see the Experimental section in the main text) by a cubic polynomial function. Q_{escape} was considered by including both natural convection and thermal radiation from the outer surface of the cell to the ambient temperature (23 ± 2 °C). Validation of the simulations is shown in Figs. S5 and S6 below, where the excellent agreement between the experimental and simulated values verifies the high reliability of the simulations.

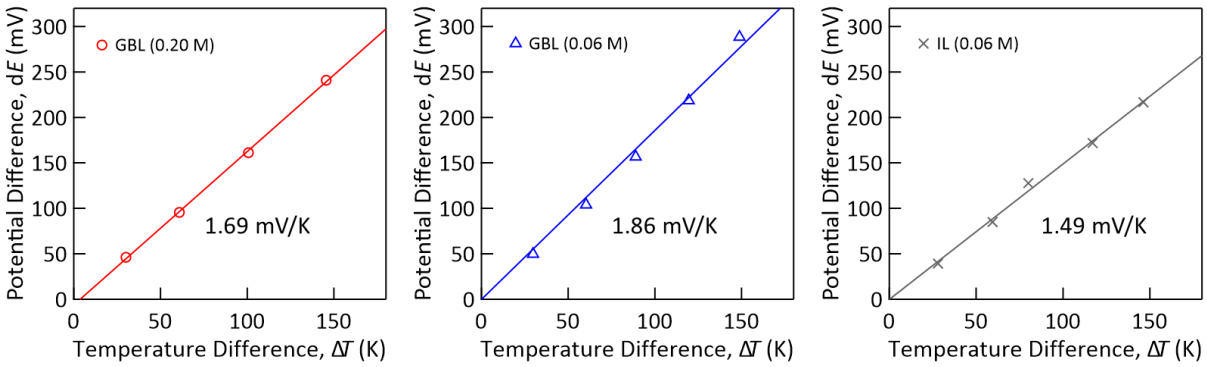

Fig. S1 Temperature dependence of the thermogalvanic voltage generated from the three electrolytes related to this study, all of which were prepared with the $Co^{II/III}(bpy)_3(NTf_2)_{2/3}$ redox couple. The measurements were conducted using our two-compartment cell with platinum wire electrodes, in which the temperature of the hot compartment (feedback controlled using a resistive heater) was varied from 50 to 170 °C while that of the cold compartment was maintained at 20 °C. The obtained Seebeck coefficients (*Se*) are summarized in Table S1. The result for $[C_2mim][NTf_2]$ ionic liquid (right panel) satisfactorily agrees with the reported value measured in the same ionic liquid ($Se \approx 1.6$ mV K^{-1}).[S2]

Table S1 Seebeck coefficients (*Se*) of the three electrolytes related to this study.

Electrolyte type (redox couple concentration)	***Se* (mV K^{-1})**
GBL (*C* = 0.20 M)	1.69
GBL (*C* = 0.06 M)	1.86
$[C_2mim][NTf_2]$ (*C* = 0.06 M)	1.49

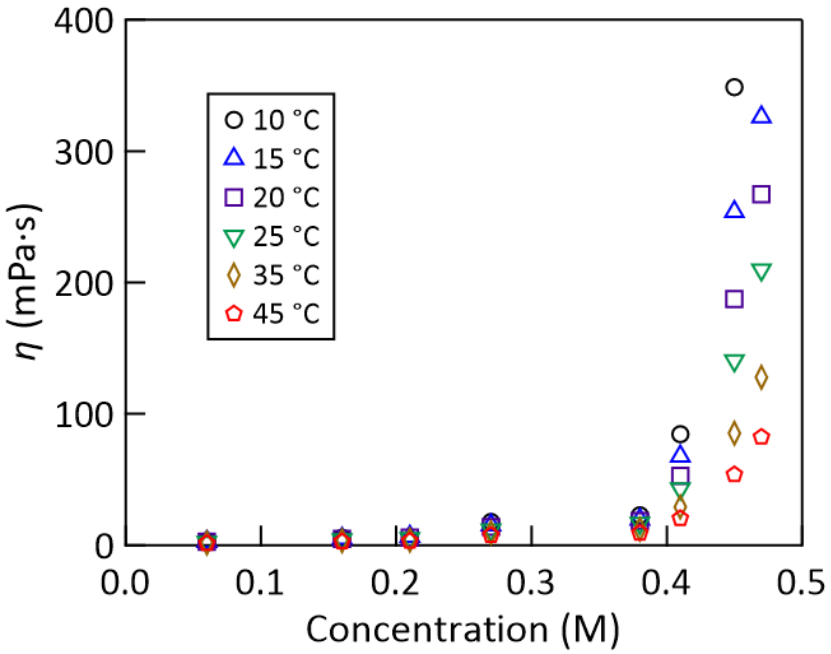

Fig. S2 Concentration dependence of the viscosity of the electrolyte. The measurements were performed for the electrolyte prepared with the $Co^{II/III}(bpy)_3(NTf_2)_{2/3}$ redox couple dissolved in GBL at different concentrations for temperatures from 10 to 45 °C. The details of the viscosity measurement are given in the Experimental section in the main text. These values are given in Table S2.

Table S2 Values of the viscosity (in mPa·s) shown in Fig. S2.

Temperature	**Concentration (M)**								
(°C)	0.0	0.06	0.16	0.21	0.27	0.38	0.41	0.45	0.47
10	2.2	3.2	5.8	7.7	18.0	23.0	84.6	349	N/A[a]
15	2.0	2.8	5.3	6.7	15.5	19.7	67.9	254	326
20	1.8	2.6	4.8	5.9	13.9	18.7	53.1	187	267
25	1.7	2.4	4.3	5.3	11.9	16.9	43.0	141	210
35	1.4	1.9	3.5	4.2	9.7	12.4	29.4	85.3	128
45	1.3	1.6	2.9	3.4	7.8	9.5	20.6	54.0	82.5

[a]Measurement could not be performed because the viscosity was too high for the rheometer used.

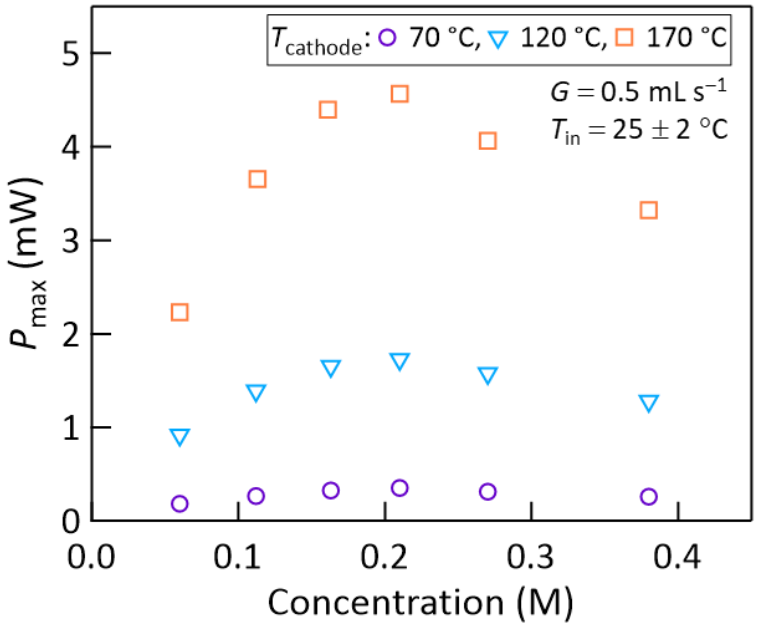

Fig. S3 Concentration dependence of the maximum power P_{max}. The measurements were performed for G = 0.5 mL s^{-1} and T_{in} = 25 ± 2 °C at the three different temperatures shown in the figure varying the concentration of the $Co^{II/III}(bpy)_3(NTf_2)_{2/3}$ redox couple in GBL. The results indicate that P_{max} has the peak at around 0.21 M. The decrease of P_{max} for higher concentration was caused by the increase of the electrolyte viscosity shown in Fig. S2.

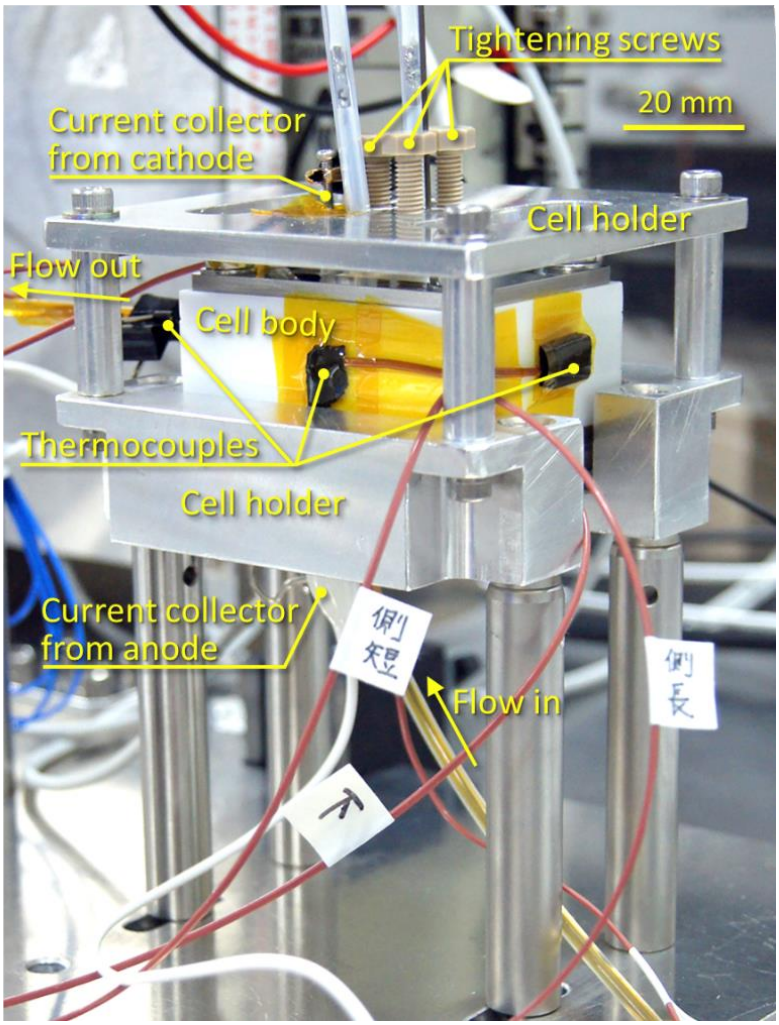

Fig. S4 Photograph of the thermocell during the experiment. The electrolyte enters from the bottom ("flow in") and leaves laterally to the left ("flow out"). Several thermocouples (brown wires) are used to measure the temperatures of the surfaces of the cell (see also the computer graphics in Fig. S5) as well as the liquid temperatures at the inlet and outlet. All of the thermocouple junctions are covered with a piece of thermal insulator (black foamed plastic) to ensure reliable measurement of the temperatures. See Fig. 2 in the main text for the details of the internal structure of the cell and our previous report[S3] for the details of the cell holder.

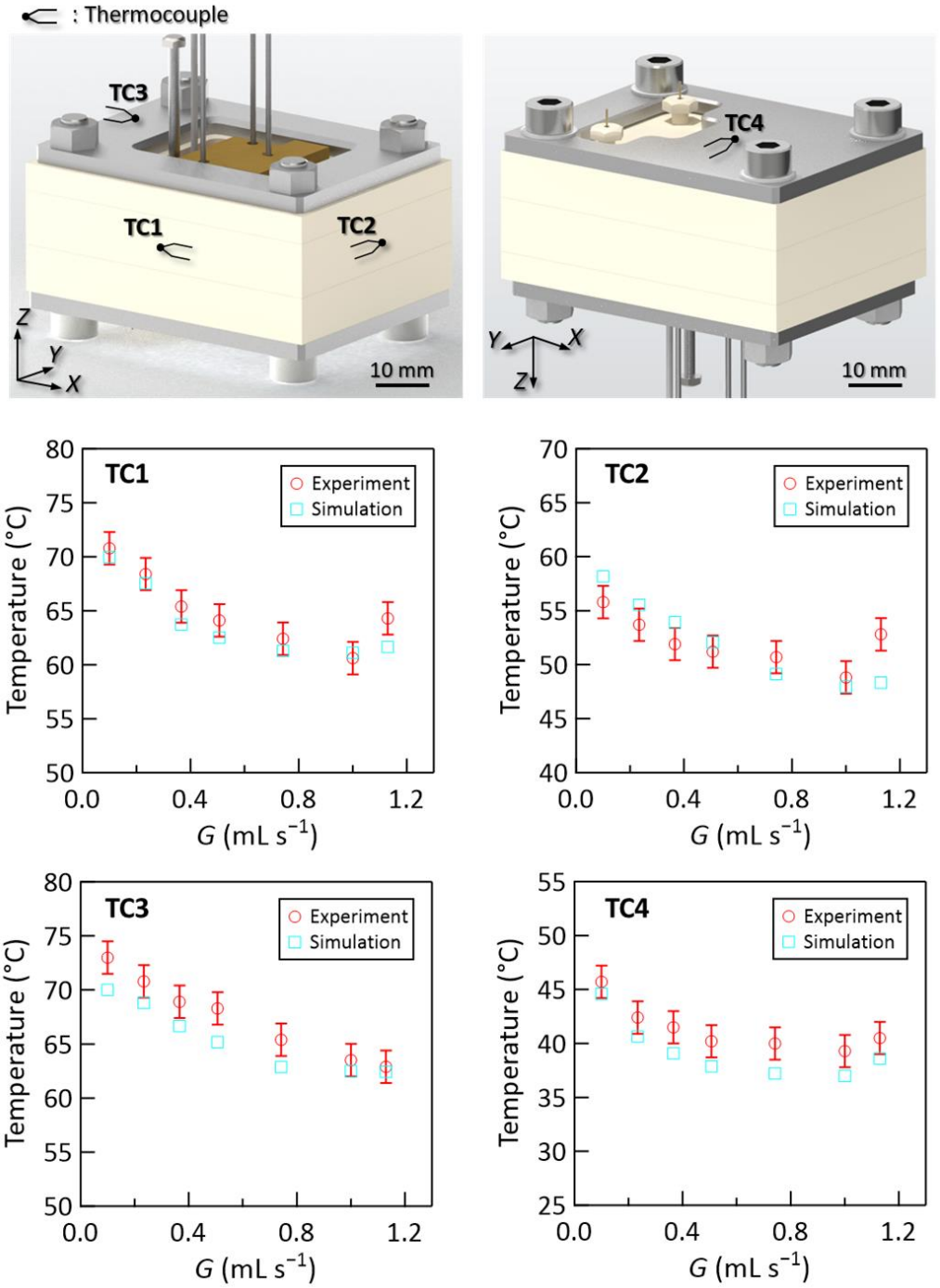

Fig. S5 Validation of the simulation in terms of the surface temperatures of the cell. Four positions on the cell surface (TC1 to TC4) were measured during the experiments, as shown in the top figures. In the four graphs, the temperatures measured with these thermocouples in the representative experiment ($T_{cathode}$ = 170 °C, T_{in} = 26 ± 4 °C, C in GBL = 0.21 M) are compared with the results from the simulations (see the Experimental section in the main text and Simulation details above in this ESI). Satisfactory agreement between the values verifies the validity of the simulations. The error bars of the experimental data (± 1.5 K) account for the uncertainty of the temperature measurements.

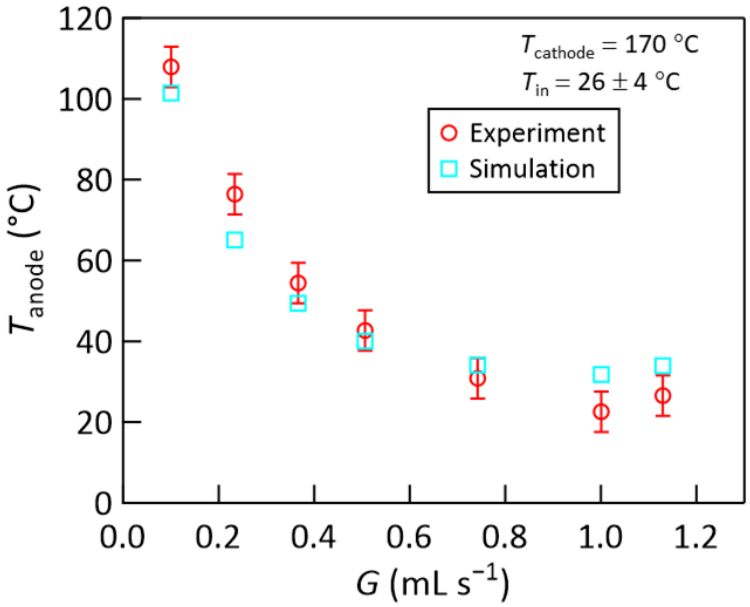

Fig. S6 Validation of the simulation in terms of the anode temperature T_{anode}. The experimental values of T_{anode} were obtained by the relationship $T_{anode} = T_{cathode} - \Delta T = T_{cathode} - V_{OC}/Se$, where V_{OC} is the open-circuit voltage shown in Fig. 4b in the main text and Se is the Seebeck coefficient shown in Table S1. The quantitative agreement between the experimental and simulation results over a wide flow rate range ($0.1 \leq G \leq 1.13$ mL s^{-1}) verifies the validity of the simulations. The error bars of the experimental data (± 5 K) account for the uncertainty arising from measurement of Se.

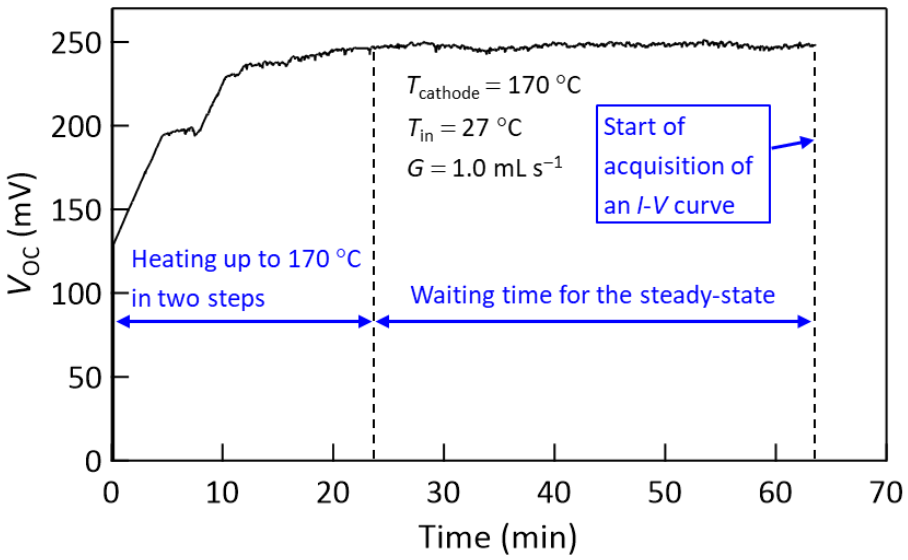

Fig. S7 Typical data of V_{OC} *vs.* time showing a stable power generation or the stability of the interelectrode temperature difference in the present cell. Experimental conditions: $T_{cathode}$ = 170 °C; T_{in} = 27 °C; G = 1.0 mL s^{-1}. This data acquisition was stopped at 63.5 min in order to start acquisition of an *I-V* curve. Note that the stability of the power generation was not limited for such a short time period but lasted at least over the entire experimental time in one experimental day, which was typically between 8 h and 15 h during which multiple datasets were acquired.

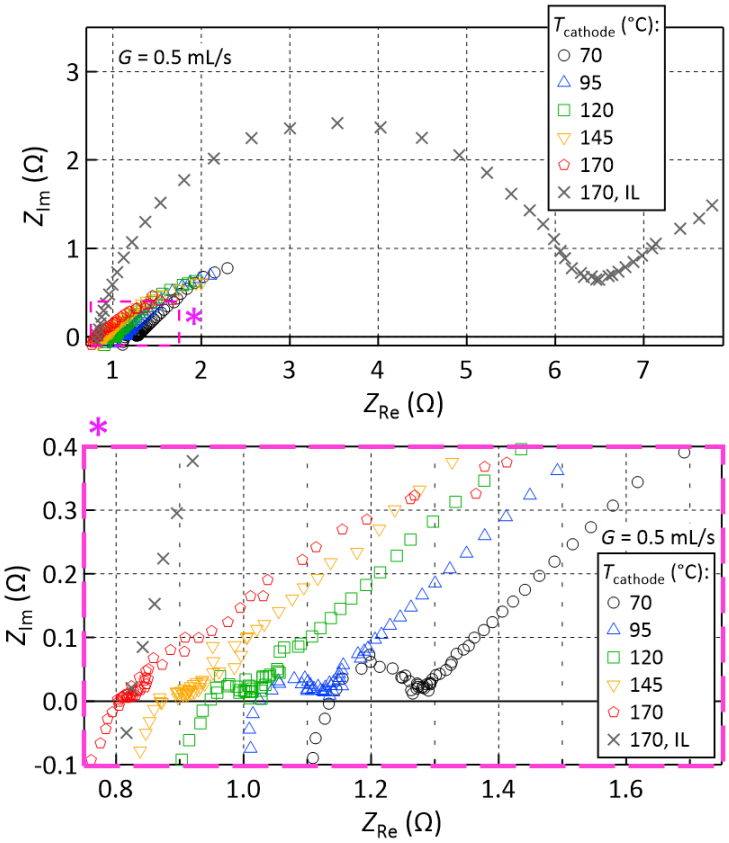

Fig. S8 Nyquist plots generated from AC impedance measurements conducted during the experiments under various cathode temperatures at the flow rate of G = 0.5 mL s^{-1}. For comparison, the data for the case of the previous electrolyte prepared with [C_2mim][NTf_2] ionic liquid (C = 0.06 M) obtained at G = 0.5 mL s^{-1} and $T_{cathode}$ = 170 °C are shown (gray crosses, from ref. S3). The bottom panel magnifies the area marked with * in the top panel.

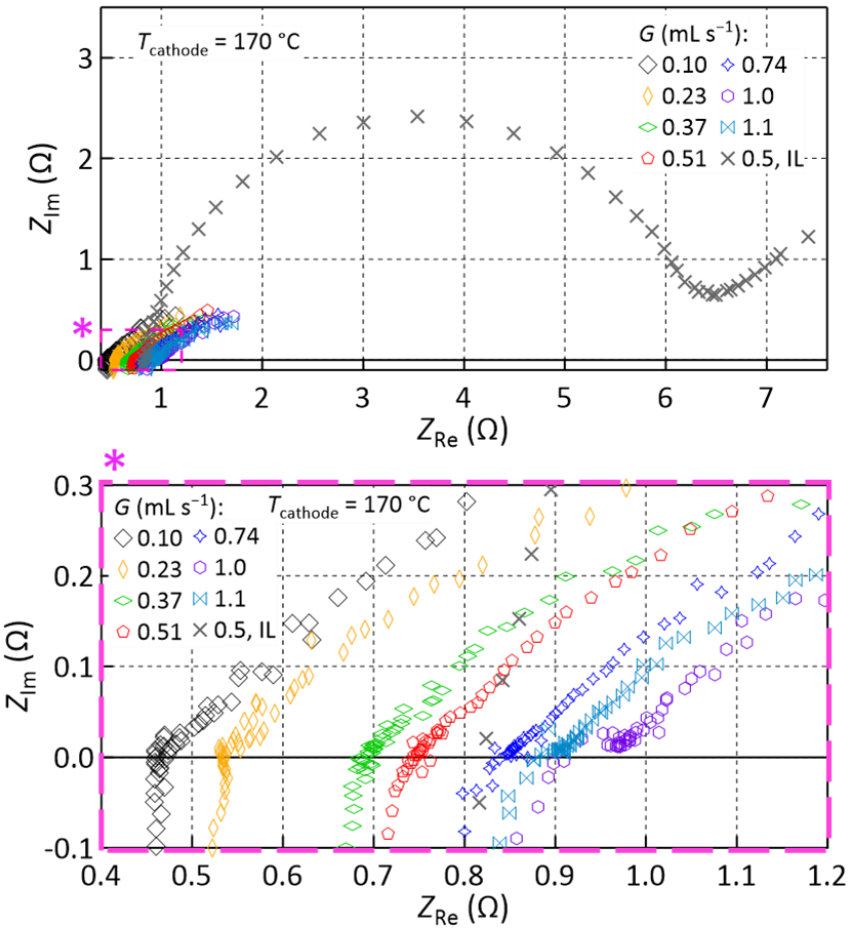

Fig. S9 Nyquist plots generated from AC impedance measurements conducted during the experiments under various flow rate at the cathode temperature of $T_{cathode}$ = 170 °C. For comparison, the data for the case of the previous electrolyte prepared with [C_2mim][NTf_2] ionic liquid (C = 0.06 M) obtained at G = 0.5 mL s^{-1} and $T_{cathode}$ = 170 °C are shown (gray crosses, from ref. S3). The bottom panel magnifies the area marked with * in the top panel.

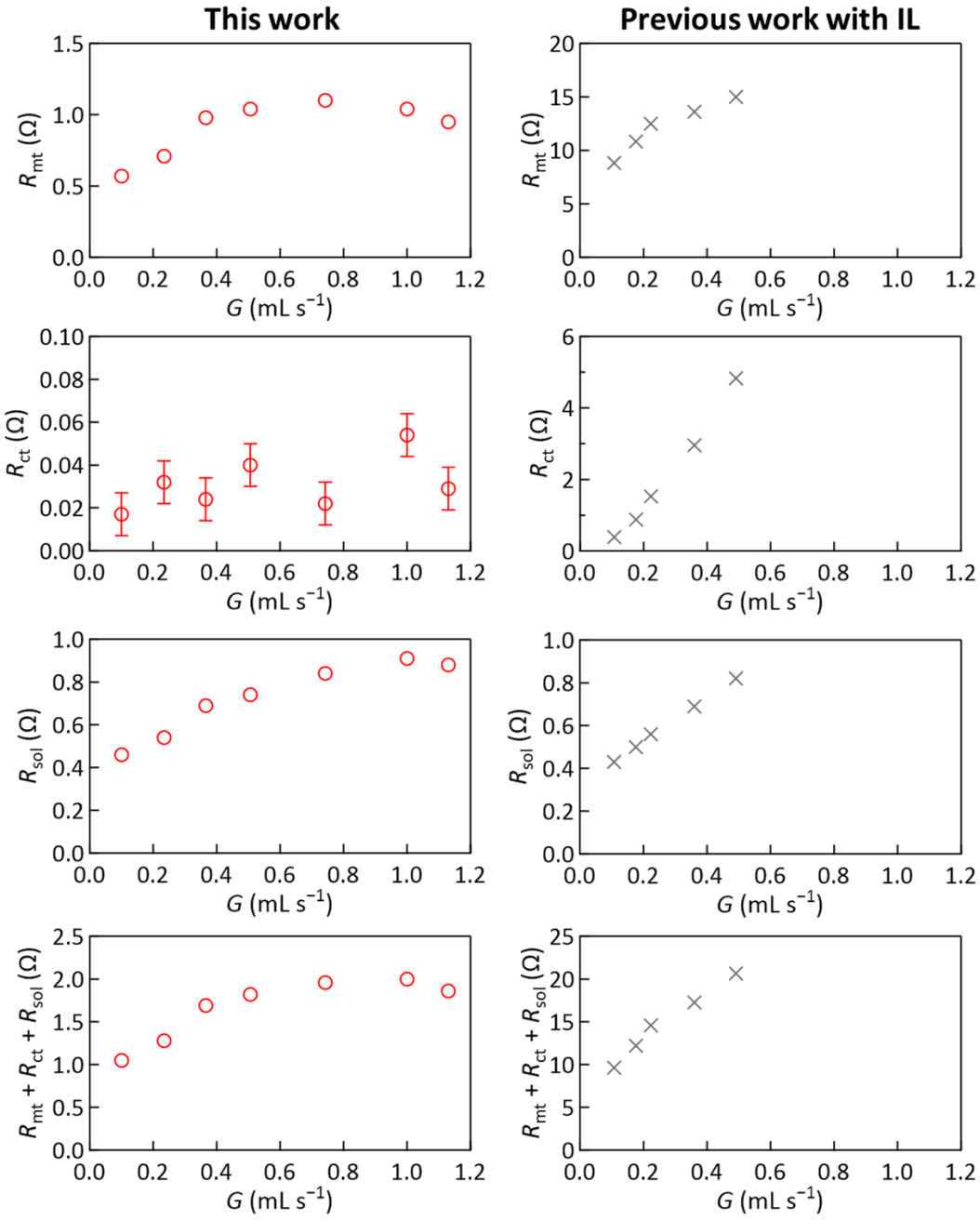

Fig. S10 Dependence of the mass-transfer resistance (R_{mt}), charge transfer resistance (R_{ct}), solution resistance (R_{sol}), and their total ($R_{mt} + R_{ct} + R_{sol}$) on the flow rate G at $T_{cathode}$ = 170 °C. The graphs on the left show the results of the present study (red circles, C = 0.21 M). The graphs on the right show the results for the ionic liquid electrolyte in our previous study (gray crosses, C = 0.06 M, from ref. S3). These resistances were determined based on the Randles equivalent circuit model[S4] (see also Fig. 3c in the main text). R_{mt} was determined using the limiting current at −400 mV and theoretical solution of R_{mt} given in ref. S3. R_{ct} and R_{sol} were determined from the Nyquist plots shown in Fig. S9. Error bars in the graph of R_{ct} for the present study represent ±0.01 Ω uncertainty in the original Nyquist plot data (see Fig. S9).

References

S1 F. Chen, Z. Yang, Z. Chen, J. Hu, C. Chen and J. Cai, *J. Mol. Liq.*, 2015, **209**, 683–692.

S2 T. J. Abraham, D. R. MacFarlane and J. M. Pringle, *Energy Environ. Sci.*, 2013, **6**, 2639–2645.

S3 Y. Ikeda, K. Fukui and Y. Murakami, *Phys. Chem. Chem. Phys.*, 2019, **21**, 25838–25848.

S4 A. J. Bard and L. R. Faulkner, *Electrochemical Methods: Fundamentals and Applications*, John Wiley & Sons, Hoboken, NJ, 2nd ed., 2001.